

# Skyrmions and anomalous Hall effect in a Dzyaloshinskii-Moriya spiral magnet

Su Do Yi,<sup>1</sup> Shigeki Onoda,<sup>2</sup> Naoto Nagaosa,<sup>3,4</sup> and Jung Hoon Han<sup>1,\*</sup>

<sup>1</sup>*Department of Physics, BK21 Physics Research Division, Sungkyunkwan University, Suwon 440-746, Korea*

<sup>2</sup>*Condensed Matter Theory Laboratory, RIKEN, 2-1 Hirosawa, Wako 351-0198, Japan*

<sup>3</sup>*Department of Applied Physics, The University of Tokyo, 7-3-1 Hongo, Bunkyo-ku, Tokyo 113-8656, Japan*

<sup>4</sup>*Cross Correlated Materials Research Group, Frontier Research System, RIKEN, 2-1 Hirosawa, Wako, Saitama 351-0198, Japan*

(Received 26 July 2009; published 25 August 2009)

Monte Carlo simulation study of a classical spin model with Dzyaloshinskii-Moriya interaction and the spin anisotropy under the magnetic field is presented. We found a rich phase diagram containing the multiple spin spiral (or Skyrme crystal) phases of square, rectangular, and hexagonal symmetries in addition to the spiral spin state. The Skyrme crystal states are stabilized by a spin anisotropy or a magnetic field. The Hall conductivity  $\sigma_{xy}$  is calculated within the *sd* model for each of the phases. Applying a magnetic field induces nonzero uniform chirality and the anomalous Hall conductivity simultaneously. The field dependence of  $\sigma_{xy}$  is shown to be a sensitive probe of the underlying magnetic structure. Relevance of the present results to several recent experiments on MnSi is discussed.

DOI: [10.1103/PhysRevB.80.054416](https://doi.org/10.1103/PhysRevB.80.054416)

PACS number(s): 75.10.Hk, 75.30.-m, 72.15.-v, 75.40.Mg

## I. INTRODUCTION

Metallic spiral magnets such as MnSi exhibit a number of intriguing phenomena that came into highlight in recent years.<sup>1-7</sup> For one, the spiral magnetic order,<sup>1,2</sup> due to the presence of Dzyaloshinskii-Moriya (DM) interaction in addition to the ferromagnetic exchange, undergoes a transformation into a partially ordered multiple spiral spin state, or a Skyrme crystal state, when pressure is applied.<sup>3</sup> A recent neutron-scattering experiment reveals that a genuine Skyrme crystal spin phase of hexagonal symmetry is stabilized in the so-called *A* phase of MnSi,<sup>7</sup> while under high pressure the diffuse neutron Bragg peaks are consistent with the cubic symmetry of multiple spiral spins.<sup>3</sup> Furthermore, following some earlier experiments by Ong's group,<sup>4,5</sup> a Hall effect of topological origin has been identified in the *A* phase of MnSi (Ref. 7) in agreement with several earlier theories relating the topological quantum number of the underlying spin texture to the anomalous Hall conductivity of conducting electrons.<sup>8-14</sup>

Several phenomenological theories have been advanced to justify the stabilization of multiple spiral spin states in magnets without the inversion symmetry.<sup>15-18</sup> And a number of papers discussed the influence of the topological spin texture carrying nonzero Skyrme number on the transverse conductivity of conducting electrons,<sup>8,9,14,19</sup> without addressing the origin of topologically nontrivial spin textures. Given the recent advances particularly with MnSi and hopefully with other metallic chiral magnets in the near future, we believe a comprehensive theoretical framework encompassing the origin of the stabilization of Skyrme crystal spin states and the anomalous Hall effect due to it is called for. In this paper, we propose such a framework wherein (i) a microscopic spin model with the DM interaction and spin anisotropy is used to deduce the existence of Skyrme crystal spin phases of both hexagonal and square symmetries in the phase diagram, and (ii) an *sd* Hamiltonian with the coupling of the local and conducting electrons' magnetic moments is used to calculate the transverse Hall conductivity  $\sigma_{xy}$  of topological origin. A

significant contribution to  $\sigma_{xy}$  is found in the Skyrme crystal phases whereas for a spiral spin state  $\sigma_{xy}$  is nearly zero. A clear and consistent connection is drawn between the underlying topological spin structure, and its manifestation in an anomalous Hall transport.

The paper is organized as follows: in Sec. II, a lattice model containing ferromagnetic exchange, Dzyaloshinskii-Moriya, and various anisotropy terms are written down and its phase diagram is examined by means of classical Monte Carlo method. A brief Ginzburg-Landau argument related to various Skyrme crystal phases we find from Monte Carlo study is presented. Finally, a variational energy calculation comparing the energies of several spiral spin configurations and the Skyrme crystal state is presented. In Sec. III, the *sd* Hamiltonian is employed to compute the Hall conductivity in the spiral spin, and various kinds of Skyrme crystal states. Within the same Kubo-type linear-response framework, we present the longitudinal conductivity  $\sigma_{xx}$  along with the Hall conductivity  $\sigma_{xy}$  for comparison. In Sec. IV, we discuss the relevance of the present results to the recent set of experiments on MnSi and summarize.

## II. MODEL AND ITS PHASE DIAGRAM

### A. Monte Carlo calculation

A continuum Hamiltonian written by Bak and Jensen for a prototypical chiral magnet MnSi some years ago<sup>20</sup> is adapted to a lattice spin model consisting of the ferromagnetic exchange (*J*), DM interaction (*K*), anisotropy (*A*<sub>1</sub> and *A*<sub>2</sub>), and the Zeeman energy (*H*)

$$\begin{aligned}
 H_S = & -J \sum_{\mathbf{r}} \mathbf{S}_{\mathbf{r}} \cdot (\mathbf{S}_{\mathbf{r}+\hat{x}} + \mathbf{S}_{\mathbf{r}+\hat{y}} + \mathbf{S}_{\mathbf{r}+\hat{z}}) - K \sum_{\mathbf{r}} (\mathbf{S}_{\mathbf{r}} \times \mathbf{S}_{\mathbf{r}+\hat{x}} \cdot \hat{x} \\
 & + \mathbf{S}_{\mathbf{r}} \times \mathbf{S}_{\mathbf{r}+\hat{y}} \cdot \hat{y} + \mathbf{S}_{\mathbf{r}} \times \mathbf{S}_{\mathbf{r}+\hat{z}} \cdot \hat{z}) + A_1 \sum_{\mathbf{r}} ((S_{\mathbf{r}}^x)^4 + (S_{\mathbf{r}}^y)^4 \\
 & + (S_{\mathbf{r}}^z)^4) - A_2 \sum_{\mathbf{r}} (S_{\mathbf{r}}^x S_{\mathbf{r}+\hat{x}}^x + S_{\mathbf{r}}^y S_{\mathbf{r}+\hat{y}}^y + S_{\mathbf{r}}^z S_{\mathbf{r}+\hat{z}}^z) - \mathbf{H} \cdot \sum_{\mathbf{r}} \mathbf{S}_{\mathbf{r}}.
 \end{aligned} \tag{1}$$

We take a cubic lattice structure rather than the full B20 structure of MnSi (Ref. 21) largely for technical simplicity, and also because our simplified model proves to be rich enough to contain several Skyrme crystal spin phases that have so far been missed in other microscopic models of spins.<sup>22</sup> The DM vector is chosen along the bond direction rather than orthogonal to it; such a choice gives rise to a spiral spin state for small anisotropy parameters with the spins lying in a plane perpendicular to the propagation vector, as is experimentally the case for MnSi.

Monte Carlo (MC) simulated annealing procedure was employed to work out the ground states for varying anisotropy strengths ( $A_1, A_2$ ) and the field strength  $H$  oriented along the  $z$  direction:  $\mathbf{H}=H\hat{z}$ . A number of simplifications were made to save the computational cost. First, a two-dimensional (2D) rather than a three-dimensional (3D) lattice was used, based on the following Hamiltonian:

$$\begin{aligned}
 H_S = & -J \sum_{\mathbf{r}} \mathbf{S}_{\mathbf{r}} \cdot (\mathbf{S}_{\mathbf{r}+\hat{x}} + \mathbf{S}_{\mathbf{r}+\hat{y}}) - K \sum_{\mathbf{r}} (\mathbf{S}_{\mathbf{r}} \times \mathbf{S}_{\mathbf{r}+\hat{x}} \cdot \hat{x} \\
 & + \mathbf{S}_{\mathbf{r}} \times \mathbf{S}_{\mathbf{r}+\hat{y}} \cdot \hat{y}) + A_1 \sum_{\mathbf{r}} ((S_{\mathbf{r}}^x)^4 + (S_{\mathbf{r}}^y)^4 + (S_{\mathbf{r}}^z)^4) \\
 & - A_2 \sum_{\mathbf{r}} (S_{\mathbf{r}}^x S_{\mathbf{r}+\hat{x}}^x + S_{\mathbf{r}}^y S_{\mathbf{r}+\hat{y}}^y) - \mathbf{H} \cdot \sum_{\mathbf{r}} \mathbf{S}_{\mathbf{r}}. \quad (2)
 \end{aligned}$$

Although the MC simulation remains tractable in 3D for a small enough lattice size, the calculation of the  $\sigma_{xy}$  becomes prohibitively demanding for a 3D lattice. Because the realistic modulation period is very large and difficult to simulate, we also choose the ratio  $K/J=\sqrt{6}$  (Hereafter we will take  $J \equiv 1$ ) which would give  $k=2\pi/6$  in 2D without the anisotropy. Calculations were mostly carried out for  $18 \times 18$  lattice, with occasional checks on a  $30 \times 30$  lattice to ensure consistency.  $2 \times 10^5$  MC steps were used at each temperature in the annealing process. It turns out that the same ground state is found over a widely different choices of  $A_1$ , and here we present all the results for  $A_1=0.5$  without loss of generality. Once the ground state has been obtained for a given  $A_2$  and  $H$ , we analyze its structure by making the Fourier transform  $\langle \mathbf{S}_{\mathbf{k}} \rangle = \sum_{\mathbf{r}} \langle \mathbf{S}_{\mathbf{r}} \rangle e^{-i\mathbf{k} \cdot \mathbf{r}}$  of the averaged MC configurations  $\langle \mathbf{S}_{\mathbf{r}} \rangle$ , and looking at the intensity profile  $|\langle \mathbf{S}_{\mathbf{k}} \rangle|^2$ . The resulting phase diagram spanned by  $(A_2, H)$  is shown in Fig. 1.

Occupying the small  $A_2$  part is a spiral spin (SS) state characterized by a pair of Bragg peaks in  $|\langle \mathbf{S}_{\mathbf{k}} \rangle|^2$  at  $\pm \mathbf{k}$ ,  $\mathbf{k}=(k, k)$  ([11] spiral). When  $A_2$  is sufficiently large, one finds the Skyrme crystal (SC) phase constructed primarily as the superposition of two pairs of spin spirals, one with  $\mathbf{k}=(\pm k, 0)$  ([10] spiral) and the other with  $\mathbf{k}=(0, \pm k)$  ([01] spiral). Depending on whether the Bragg intensities are the same or different for the two pairs, we denote them as  $SC_1$  (nonidentical) or  $SC_2$  (identical). In practice  $SC_1$  is fragile, occupying only a tiny fraction of the phase diagram. A third class of SC state is found when the field strength in exceed of a certain threshold value  $H_c$  is applied to the SS phase. This state, denoted  $SC_h$ , is characterized by three sets of modulation vectors which are related by  $120^\circ$  rotations. The phase boundaries separating SS from either  $SC_h$  or  $SC_1$  are first order.

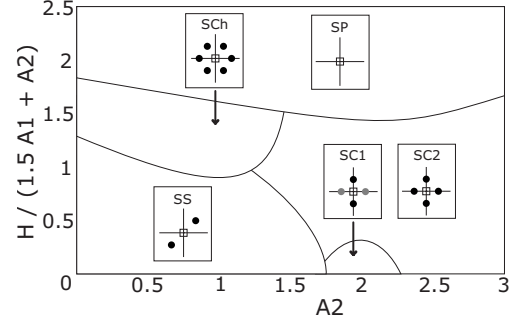


FIG. 1. Low temperature ( $T=0.01$ ) phase diagram of the spin model in Eq. (2) (2D version) with  $K=\sqrt{6}$ ,  $A_1=0.5$ , and  $\mathbf{H}=H\hat{z}$ . Phase boundaries are drawn on the basis of MC simulations at a large number of  $(A_2, H)$  locations. Spin configurations are abbreviated as SS (spiral spin), and SC (spin crystal). Full spin polarization (SP) results at high field. The Skyrme crystal phases are further classified as  $SC_1$  (unequal Bragg intensities),  $SC_2$  (equal Bragg intensities), and  $SC_h$  (hexagonal Bragg spots). The corresponding Bragg patterns are schematically shown. The Bragg peak at  $\mathbf{k}=0$  emerges due to the field-induced uniform magnetization. On the vertical axis  $H$  is divided by an arbitrary energy scale  $1.5A_1 + A_2$  for improved clarity of the plot.

The projection of spin patterns onto the  $xy$  plane is displayed in Fig. 2 for the three SC states. We introduce the local chirality  $\chi_{\mathbf{r}}$  at the lattice site  $\mathbf{r}$  as

$$8\pi\chi_{\mathbf{r}} = \mathbf{S}_{\mathbf{r}} \cdot (\mathbf{S}_{\mathbf{r}+\hat{x}} \times \mathbf{S}_{\mathbf{r}+\hat{y}}) + \mathbf{S}_{\mathbf{r}} \cdot (\mathbf{S}_{\mathbf{r}-\hat{x}} \times \mathbf{S}_{\mathbf{r}-\hat{y}}). \quad (3)$$

It is well-known that a single localized Skyrmion would give the uniform chirality  $\chi = \sum_{\mathbf{r}} \chi_{\mathbf{r}}$  equal to unity in the continuum limit. Plots of  $\chi_{\mathbf{r}}$  in Fig. 2 for several representative SC spin configurations clearly display the presence of Skyrmion (bright) and anti-Skyrmion (dark) regions. The Skyrmion density map is largely one-dimensional for  $SC_1$ , checkerboardlike for  $SC_2$ , and hexagonal for  $SC_h$ . Upon thermal averaging over more than  $10^4$  spin configurations, the averaged uniform chirality  $\langle \chi \rangle$  is found to be identically zero for all the spin states obtained at zero field at any temperature  $T$ .

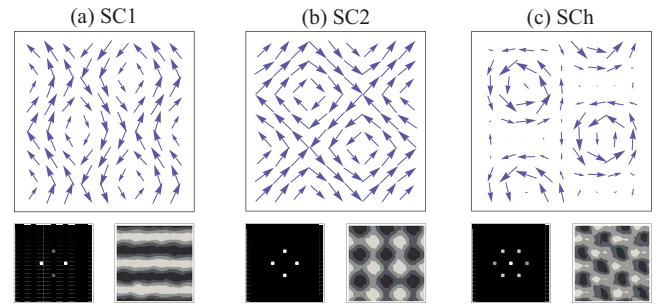


FIG. 2. (Color online) A plot of the spin configuration projected on the  $xy$  plane ( $S_i^x, S_i^y$ ) in the three spin crystal ground states: (a)  $SC_1$  at  $(A_2, H)=(2.0, 0.0)$ , (b)  $SC_2$  at  $(A_2, H)=(3.0, 0.0)$ , and (c)  $SC_h$  at  $(A_2, H)=(0.0, 2.0)$ . At the bottom left of each figure are the plots of the Bragg intensity  $|\langle \mathbf{S}_{\mathbf{k}} \rangle|^2$  showing two ( $SC_1, SC_2$ ) and three ( $SC_h$ ) sets of modulation vectors. Shown at the bottom right are the plots of the local chirality  $\chi_{\mathbf{r}}$ . Bright (dark) regions correspond to Skyrmions (anti-Skyrmions).

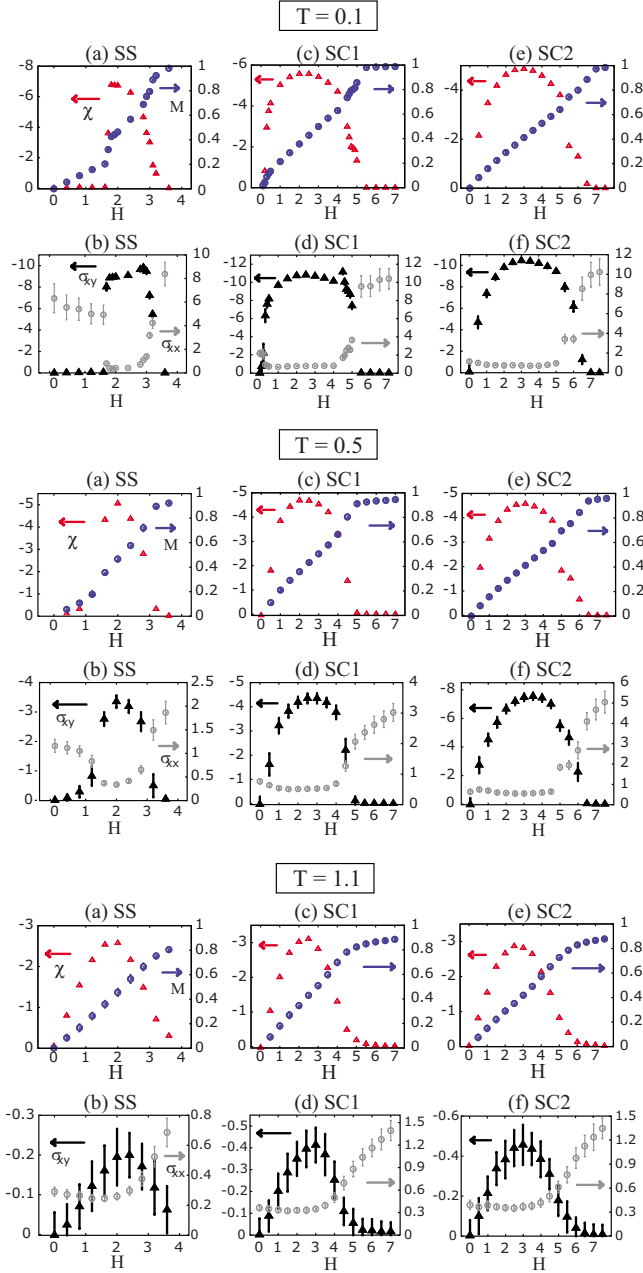


FIG. 3. (Color online) Upper panels: plot of uniform magnetization  $\langle M \rangle$  (blue circle) and uniform chirality  $\langle \chi \rangle$  (red triangle) with varying field strength  $H$ ,  $\mathbf{H}=H\hat{z}$ , for (a) SS at  $(A_1, A_2)=(0.5, 0.0)$ , (c) SC<sub>1</sub> at  $(A_1, A_2)=(0.5, 2.0)$ , and (e) SC<sub>2</sub> at  $(A_1, A_2)=(0.5, 3.0)$ , at three temperatures  $T=0.1$  (top six figures), 0.5 (middle), and 1.1 (bottom). Lower panels:  $\langle \sigma_{xy} \rangle$  averaged over 100 MC-generated spin configurations are shown in (b), (d), and (f) at corresponding temperatures and field strengths. Thermal fluctuations are indicated as error bars. Thermal-averaged  $\langle \sigma_{xx} \rangle$  are shown in gray for comparison.

### B. Ginzburg-Landau consideration

With the magnetic field along the  $z$  direction turned on, the uniform chirality becomes nonzero as shown in Fig. 3. A stark contrast in the field dependence of the chirality arises depending on whether the one-dimensional ground state is SS or SC. For the former, nonzero  $\chi$  does not appear until a

threshold field  $H_c$  is reached and the hexagonal Skyrme crystal SC<sub>*h*</sub> state realized. For the SC ground state, however, the onset of nonzero chirality is immediate with the field. The same field dependence is found for the magnetic field oriented away from the  $z$  direction. Hence it is seen that the chirality and, as will be seen shortly, the anomalous Hall conductivity, serves as a sensitive probe of the underlying spin structure being a single or a multiple spiral. Nonzero uniform chirality is realized when the triple product  $\mathbf{S}_{\mathbf{k}_1+\mathbf{k}_2}^* \cdot \mathbf{S}_{\mathbf{k}_1} \times \mathbf{S}_{\mathbf{k}_2}$  becomes nonzero,  $\mathbf{S}_{\mathbf{k}}$  being the Fourier component of the spin configuration. For the SC<sub>*h*</sub> the three independent modulation vectors naturally satisfy  $\mathbf{S}_{\mathbf{k}_1+\mathbf{k}_2}^* \cdot \mathbf{S}_{\mathbf{k}_1} \times \mathbf{S}_{\mathbf{k}_2} \neq 0$  and give rise to the chirality. For the SC<sub>1</sub> or SC<sub>2</sub> states, we find that it is the triple product  $\mathbf{S}_{\mathbf{k}_x+\mathbf{k}_y}^* \cdot \mathbf{S}_{\mathbf{k}_x} \times \mathbf{S}_{\mathbf{k}_y}$ , with  $\mathbf{k}_x=(k, 0)$  and  $\mathbf{k}_y=(0, k)$ , which is responsible for the chirality. The higher harmonic  $\mathbf{S}_{\mathbf{k}_x+\mathbf{k}_y}^*$  is induced by the magnetic field and its amplitude grows with  $H$ , and therefore  $\chi \sim H$  for small  $H$  as seen in Fig. 3.

### C. Variational energy calculation

A number of recipes for the realization of multiple spiral spin structures have been proposed in the past,<sup>15–18</sup> but none has emphasized the possible role of the spin anisotropy such as  $A_2$  in stabilizing SC order. We have compared the energy of the [11]-spiral spins with that of the [10]-spiral spin state as well as the SC<sub>2</sub> state. For the two spiral spin states we use the configuration

$$\mathbf{S}_{\mathbf{r}}^{[11]} = \left( -\frac{1}{\sqrt{2}} \cos[k(x_i + y_i)], \frac{1}{\sqrt{2}} \cos[k(x_i + y_i)], \sin[k(x_i + y_i)] \right),$$

$$\mathbf{S}_{\mathbf{r}}^{[10]} = (0, \cos[kx_i], \sin[kx_i]). \quad (4)$$

The spin configuration for the 2D Skyrme crystal state is chosen as the superposition of two right-handed spiral spins

$$\mathbf{S}_{\mathbf{r}} = A \left( 0, \cos(kx_i + \alpha), \frac{1}{2} \sin(kx_i + \alpha) \right) + A \left( \sin(ky_i + \beta), 0, \frac{1}{2} \cos(ky_i + \beta) \right). \quad (5)$$

The factor 1/2 in the  $z$  component is dictated by the detailed analysis of the ground-state SC<sub>2</sub> spin configuration obtained from Monte Carlo study, which revealed that the  $z$  component is only half the size of the  $x$  or the  $y$  component of the underlying spiral spins. This should be due to the two dimensionality of the lattice, which can make a distinction between the  $z$  direction and the other two directions. For the 3D case we do not expect such an anisotropy to exist. The factor  $A$  is  $2/\sqrt{5}$  to ensure  $(1/N)\sum_{\mathbf{r}} \mathbf{S}_{\mathbf{r}}^2 = 1$ . In effect, we are replacing the local constraint  $\mathbf{S}_{\mathbf{r}}^2 = 1$  by a global one in writing down the above variational Skyrme crystal spin configuration.

With these spin configurations the energy per spin reads

$$E_{[11]} = -2J \cos k - \sqrt{2}K \sin k + \frac{9}{16}A_1 - \frac{1}{2}A_2 \cos k,$$

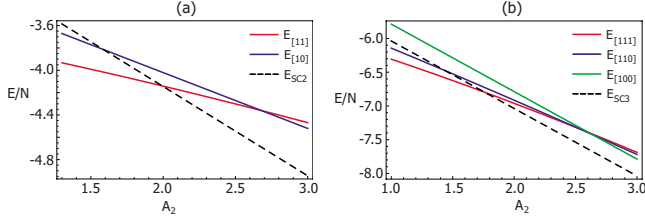


FIG. 4. (Color online) (a) Plot of the energies of spiral spins and Skyrme crystal spins in 2D for  $J=1$ ,  $K=\sqrt{6}$ ,  $A_1=0.5$ , and varying  $A_2$ . (b) Plot of the energies of spiral spins and Skyrme crystal spins in 3D for  $J=1$ ,  $K=3$ ,  $A_1=0.5$ , and varying  $A_2$ . In both instances the Skyrme crystal spin configuration becomes the lowest in energy for  $A_2$  exceeding a certain critical value.

$$E_{[10]} = -J(1 + \cos k) - K \sin k + \frac{3}{4}A_1 - \frac{1}{2}A_2,$$

$$E_{SC_2} = -J(1 + \cos k) - \frac{4}{5}K \sin k + \frac{51}{100}A_1 - \frac{4}{5}A_2. \quad (6)$$

Once the energy expressions are minimized with respect to  $k$ , we obtain

$$\tan k_{[111]} = \frac{\sqrt{2}K}{2J + \frac{1}{2}A_2}, \tan k_{[110]} = \frac{K}{J}, \tan k_{SC_2} = \frac{4K}{5J}, \quad (7)$$

for the modulus of the wave vectors and

$$E_{[111]} = -\sqrt{\left(2J + \frac{1}{2}A_2\right)^2 + 2K^2} + \frac{9}{16}A_1,$$

$$E_{[110]} = -J - \sqrt{J^2 + K^2} + \frac{3}{4}A_1 - \frac{1}{2}A_2,$$

$$E_{SC_2} = -J - \sqrt{J^2 + \frac{16}{25}K^2} + \frac{51}{100}A_1 - \frac{4}{5}A_2, \quad (8)$$

for the energies. Compared with the expressions of the energy for [11]- and [10]-spiral spins, the energy of the 2D SC state decreases with  $A_2$  with the slope  $4/5$  which is greater than the slope  $1/2$  for the spiral spins. Hence the SC phase eventually will win out over the spiral spin states for sufficiently large  $A_2$ . However, the two phase angle  $\alpha$  and  $\beta$  are not fixed in this way. It is probably necessary to introduce the fourth-order interaction terms to resolve the phase angles.

Variationally obtained energies are plotted in Fig. 4(a) for a fixed set of  $J, K, A_1$  and varying  $A_2$ . The energy of the Skyrme crystal state  $E_{SC_2}$  becomes the lowest when  $A_2 \gtrsim 2.0$ , not far from the MC result of  $A_2 \gtrsim 2.25$ . In view of the pressure-induced realization of the isotropic, multiple spiral states in MnSi,<sup>3</sup> our findings here can be interpreted as the effect of pressure and the resulting isotropy being faithfully reflected in our model as the increased value of  $A_2$ . Realization of  $SC_h$  phase requires the magnetic field instead, and experimentally the  $A$  phase where a similar spin structure was found in MnSi occurs at ambient pressure, again supporting the connection of  $A_2$  with pressure.

Next we turn to the 3D spiral spins oriented along [111], [110], and [100] directions, and calculate their energies using the 3D spin Hamiltonian given in Eq. (1). The spin configuration for the [111] direction is given by

$$\mathbf{S}_r^{[111]} = \cos[k(x_i + y_i + z_i)]\hat{e}_1 + \sin[k(x_i + y_i + z_i)](\hat{k} \times \hat{e}_1) \quad (9)$$

where  $\hat{e}_1$  is an arbitrary unit vector lying in the plane orthogonal to [111]. Spins oriented along [100] and [110] are already given in Eq. (4). For the 3D Skyrme crystal spins we take the variational spin-configuration

$$\mathbf{S}_r^{SC_3} = A[0, \cos(kx_i + \alpha), \sin(kx_i + \alpha)] + A[\sin(ky_i + \beta), 0, \cos(ky_i + \beta)] + A[\cos(kz_i + \gamma), \sin(kz_i + \gamma), 0]. \quad (10)$$

The factor  $A$  is  $1/\sqrt{3}$  to ensure  $(1/N)\sum_i \mathbf{S}_i^2 = 1$ . With these expressions for spins, the energies per spin can be written as

$$E_{[111]} = -3J \cos k - \sqrt{3}K \sin k + \frac{1}{2}A_1 - A_2 \cos k,$$

$$E_{[110]} = -J(1 + 2 \cos k) - \sqrt{2}K \sin k + \frac{9}{16}A_1 - \frac{1}{2}A_2(1 + \cos k),$$

$$E_{[100]} = -J(2 + \cos k) - K \sin k + \frac{3}{4}A_1 - A_2,$$

$$E_{SC_3} = -J(2 + \cos k) - K \sin k + \frac{1}{4}A_1 - A_2. \quad (11)$$

Once we optimize for  $k$ , the modulus of  $k$  vectors and energies read

$$\tan k_{[111]} = \frac{\sqrt{3}K}{3J + A_2}, \tan k_{[110]} = \frac{\sqrt{2}K}{2J + A_2/2},$$

$$\tan k_{[100]} = \frac{K}{J}, \tan k_{SC_3} = \frac{K}{J}, \quad (12)$$

and

$$E_{[111]} = -\sqrt{(3J + A_2)^2 + 3K^2} + \frac{1}{2}A_1,$$

$$E_{[110]} = -J - \sqrt{\left(2J + \frac{1}{2}A_2\right)^2 + 2K^2} + \frac{9}{16}A_1 - \frac{1}{2}A_2,$$

$$E_{[100]} = -2J - \sqrt{J^2 + K^2} + \frac{3}{4}A_1 - A_2,$$

$$E_{SC_3} = -2J - \sqrt{J^2 + K^2} + \frac{1}{4}A_1 - A_2. \quad (13)$$

Energies are plotted in Fig. 4(b) for a fixed set of  $J, K, A_1$  and varying  $A_2$ .

In both 2D and 3D calculations, we learn that the spiral spins eventually give way to the Skyrme crystal spins in energy for a sufficiently large anisotropy parameter  $A_2$ . It should be mentioned that although we did look for the 3D Skyrmonic ground states in the spin model (1) in the parameter range where, according to Fig. 4, one might expect the Skyrme crystal to exist, there was no indication of such a state being realized at low temperature. The discrepancy might be due to the soft constraint  $(\sum_i \mathbf{S}_i^2)/N=1$  used in the variational calculation that replaces the ‘‘hard constraint’’  $\mathbf{S}_i^2=1$  followed in the Monte Carlo simulation. We leave it as an interesting future exercise to look for the full 3D Skyrme crystal configuration in some sort of spin model.

### III. ANOMALOUS HALL CONDUCTIVITY

Having studied the magnetic phase diagram, we turn to the coupling of the local moments to the conduction electrons that would result in the anomalous Hall effect. We adopt the *sd* Hamiltonian

$$H = -t \sum_{\mathbf{r}\mathbf{r}'\sigma} c_{\mathbf{r}\sigma}^+ c_{\mathbf{r}'\sigma} - \lambda \sum_{\mathbf{r}} \mathbf{S}_{\mathbf{r}} \cdot c_{\mathbf{r}\alpha}^+ (\boldsymbol{\sigma})_{\alpha\beta} c_{\mathbf{r}\beta}, \quad (14)$$

with the moment distribution  $\{\mathbf{S}_{\mathbf{r}}\}$  obtained from previous MC calculation. The intrinsic anomalous Hall conductivity  $\sigma_{xy}$  in the static limit is calculated from the Kubo formula<sup>23</sup>

$$\sigma_{xy} = \frac{2\pi}{L^2} \sum_{m \neq n} \frac{f_n - f_m}{\eta^2 + (\epsilon_m - \epsilon_n)^2} \text{Im}(\langle m | J_x | n \rangle \langle n | J_y | m \rangle) \quad (15)$$

expressed in units of  $e^2/h$ . The sum  $\sum_{m \neq n}$  extends over all nonidentical pairs of single-particle eigenstates of Eq. (14),  $f_m$  is the Fermi function  $1/(e^{\beta\epsilon_m} + 1)$ , and  $L^2$  gives the number of lattice sites.  $J_x$  and  $J_y$  are the current operators. The same temperature  $T$  is used both in the Monte Carlo generation of sample spin configurations, and in evaluating  $\sigma_{xy}$ . Thermal average  $\langle \sigma_{xy} \rangle$  was taken over 100 MC-generated spin configurations. The relaxation rate  $\eta=0.1$ , and the *sd* coupling  $\lambda=1$  were used in the calculation, with similar results at other parameter choices. Since the relativistic spin-orbit coupling term is absent in Eq. (14), the nonzero Hall conductivity we will report below can only be due to the topological Berry phase effects.

We find  $\langle \sigma_{xy} \rangle = 0$ , as well as  $\langle \chi \rangle = 0$ , for all the spin configurations at all temperatures when  $H=0$ . For finite fields, on the other hand, the onset of nonzero  $\langle \sigma_{xy} \rangle$  and nonzero  $\langle \chi \rangle$  coincided almost perfectly, confirming the earlier theoretical anticipation that an unconventional anomalous Hall conductivity arises as a consequence of nonzero uniform spin chirality.<sup>8-14,19,23</sup> We also verified  $\langle \sigma_{xy} \rangle \propto \langle \chi \rangle$  when both are sufficiently small. Such a close tie between  $\langle \chi \rangle$  and  $\langle \sigma_{xy} \rangle$  revealed in our calculation suggests that measurement of  $\sigma_{xy}$  can be used as an effective probe of the underlying spin structure.

The field dependence of uniform magnetization  $\langle M \rangle = \sum_i \langle S_i^z \rangle / L^2$ , along with  $\langle \chi \rangle$  and  $\langle \sigma_{xy} \rangle$ , are displayed in Fig. 3 for several temperatures. Under the full polarization at high field where  $\langle M \rangle = 1$ ,  $\langle \chi \rangle$  and hence  $\langle \sigma_{xy} \rangle$  must go to zero, resulting in the characteristic dome shape of the  $\langle \sigma_{xy}(H) \rangle$  curve. The low-temperature  $\langle \sigma_{xy} \rangle$  can reach up to  $\approx 10e^2/h$ , similar to the value reported in an earlier model calculation.<sup>14</sup> Although the uniform chirality in the continuum limit should take on integer-only values,<sup>19</sup> the finite-size lattice result we present with nonsmoothly varying spins does not have to yield a quantized  $\langle \chi \rangle$ . For the  $SC_2$  ground state, in particular, the nonzero chirality can be phrased as  $\chi \sim \mathbf{H} \cdot \mathbf{S}_{\mathbf{k}_x} \times \mathbf{S}_{\mathbf{k}_x}$ , namely, as a quantity coupled to the vector spin chirality.<sup>24</sup> In Ref. 24, however, the influence of the external magnetic field was neglected and thus they did not obtain a nonzero Hall conductivity as we do.

For completeness, we also calculated the longitudinal conductivity using the Kubo formula

$$\sigma_{xx} = \frac{2\pi}{L^2} \eta \sum_{m \neq n} \frac{f_n - f_m}{\epsilon_m - \epsilon_n} \frac{|\langle m | J_x | n \rangle|^2}{\eta^2 + (\epsilon_m - \epsilon_n)^2}. \quad (16)$$

Thermal averages over 100 MC configurations are shown in Fig. 3 along with  $\langle \sigma_{xy} \rangle$  for comparison. The surprising and interesting feature is that the rise of  $\langle \sigma_{xy} \rangle$  is closely correlated with a rather sharp drop in the value of  $\langle \sigma_{xx} \rangle$ . In order to ensure that this effect is not an artifact of the numerics, we evaluated  $\langle \sigma_{xx} \rangle$  and  $\langle \sigma_{xy} \rangle$  for three different values of the relaxation parameter  $\eta$ , and they all maintained the same qualitative features. A natural explanation of the suppression of conductivity  $\langle \sigma_{xx} \rangle$  would be that the electronic states are depleted near the Fermi level due to the opening of a gap. However, an inspection of the energy levels obtained shows absolutely no sign of a gap opening. Instead, we find almost no variation in the electronic density of states between the spiral spin and the Skyrme crystal spin configurations. At the moment we suspect that the enlargement of the magnetic unit cell from  $(\lambda/a)$  to  $(\lambda/a)^2$ , where  $\lambda/a$  reflects the spiral modulation period measured in units of the lattice constant, in going from a single spiral to a multiple spiral phase, may explain the reduced longitudinal conductivity in the SC phase. Further investigation of the localization properties of the eigenstates will be required to completely resolve the issue. In Ref. 5, a kinklike feature in the longitudinal resistance coinciding with the system’s entry into the state exhibiting the anomalous Hall effect was observed. By converting the calculated  $\sigma_{xx}$  and  $\sigma_{xy}$  to the resistance, we were able to reproduce such kinklike features.

### IV. CONCLUSION AND SUMMARY

Despite the considerable simplifications assumed in our model calculation, there are a number of unmistakable similarities of our results to the recent set of data for MnSi. The first-order collapse of the magnetic ordering temperature  $T_c$  at the critical pressure and the reorientation of the main Bragg peak from [111] to [110] in MnSi (Ref. 3) is consistent with the first-order change with  $A_2$  in going from SS to SC phase and the reorientation of the primary ordering vector

from [11] to [10] direction in our model. Through a model calculation we showed that a more isotropic Skyrme crystal state is favored by a larger anisotropy  $A_2$ , while experimentally it is the pressure that must favor the isotropic spin states. A recent observation of the hexagonal Bragg spots in the  $A$  phase of MnSi (Ref. 6) is clearly in accord with the  $SC_h$  found in our spin model. In both instances, a finite magnetic field is needed to turn a spiral spin into a triple spiral phase. The measurement of Hall effect in the  $A$  phase was interpreted in terms of the nonzero topological quantum number carried by the hexagonal Skyrme crystal state.<sup>7</sup> In particular, the rather sharp appearance of the extra Hall signal upon entering into the  $A$  phase<sup>7</sup> can be readily understood by referring to the sudden rise in  $\langle\sigma_{xy}\rangle$  as  $H$  exceeds the threshold value  $H_c$  in Fig. 3(b).

To summarize, a simple microscopic spin model under the influence of spin anisotropy and magnetic field was shown to give rise to several multiple spiral spin ground states. The anomalous Hall conductivity for all these spin configurations under the magnetic field was calculated using the  $sd$  Hamiltonian. A number of observations concerning the magnetic structures and the anomalous Hall effect made in our paper are found to be in good accord with the recent data on MnSi.

The strategy of our approach to chiral magnetism, of which MnSi is one of the best examples, consists of two steps. The first step is in writing down a reasonable effective model which describes the known phases such as the recently observed hexagonal Skyrme crystal state in the  $A$  phase of MnSi. Our microscopic spin model successfully captures this phase, and should be considered complementary to the phenomenological approach adopted by others.<sup>6</sup>

#### ACKNOWLEDGMENTS

N.N. is supported by Grant-in-Aids under the Grants No. 16076205, No. 17105002, No. 19019004, and No. 19048015 from the Ministry of Education, Culture, Sports, Science and Technology of Japan. S.O. is supported by Grants-in-Aid for Scientific Research Grants No. 20029006 and No. 20046016 from the MEXT of Japan and Grant No. 21740275 from the JSPS. H.J.H. is supported by the Korea Research Foundation Grant (Grants No. KRF-2008-521-C00085 and No. KRF-2008-314-C00101) and in part by the Asia Pacific Center for Theoretical Physics. H.J.H. thanks A. Rosch for critical comments on the initial draft, and U. K. Rößler and A. N. Bogdanov for an interesting conversation on the subject.

\*hanjh@skku.edu

<sup>1</sup>Y. Ishikawa, K. Tajima, D. Bloch, and M. Roth, *Solid State Commun.* **19**, 525 (1976).

<sup>2</sup>C. Thessieu, C. Pfleiderer, A. N. Stepanov, and J. Flouquet, *J. Phys.: Condens. Matter* **9**, 6677 (1997).

<sup>3</sup>C. Pfleiderer, D. Reznik, L. Pintschovius, H. v. Löhneysen, M. Garst, and A. Rosch, *Nature (London)* **427**, 227 (2004).

<sup>4</sup>Minhyea Lee, Y. Onose, Y. Tokura, and N. P. Ong, *Phys. Rev. B* **75**, 172403 (2007).

<sup>5</sup>Minhyea Lee, W. Kang, Y. Onose, Y. Tokura, and N. P. Ong, *Phys. Rev. Lett.* **102**, 186601 (2009).

<sup>6</sup>S. Mühlbauer, B. Binz, F. Joinetz, C. Pfleiderer, A. Rosch, A. Neubauer, R. Georgii, and P. Böni, *Science* **323**, 915 (2009).

<sup>7</sup>A. Neubauer, C. Pfleiderer, B. Binz, A. Rosch, R. Ritz, P. G. Niklowitz, and P. Böni, *Phys. Rev. Lett.* **102**, 186602 (2009).

<sup>8</sup>J. Ye, Y. B. Kim, A. J. Millis, B. I. Shraiman, P. Majumdar, and Z. Tesanovic, *Phys. Rev. Lett.* **83**, 3737 (1999).

<sup>9</sup>S. H. Chun, M. B. Salamon, Y. Lyanda-Geller, P. M. Goldbart, and P. D. Han, *Phys. Rev. Lett.* **84**, 757 (2000); Y. Lyanda-Geller, S. H. Chun, M. B. Salamon, P. M. Goldbart, P. D. Han, Y. Tomioka, A. Asamitsu, and Y. Tokura, *Phys. Rev. B* **63**, 184426 (2001).

<sup>10</sup>K. Ohgushi, S. Murakami, and N. Nagaosa, *Phys. Rev. B* **62**, R6065 (2000).

<sup>11</sup>Y. Taguchi, Y. Oohara, H. Yoshizawa, N. Nagaosa, and Y.

Tokura, *Science* **291**, 2573 (2001).

<sup>12</sup>G. Tatara and H. Kawamura, *J. Phys. Soc. Jpn.* **71**, 2613 (2002).

<sup>13</sup>S. Onoda and N. Nagaosa, *Phys. Rev. Lett.* **90**, 196602 (2003).

<sup>14</sup>P. Bruno, V. K. Dugaev, and M. Taillefumier, *Phys. Rev. Lett.* **93**, 096806 (2004); G. Metalidis and P. Bruno, *Phys. Rev. B* **74**, 045327 (2006).

<sup>15</sup>S. Tewari, D. Belitz, and T. R. Kirkpatrick, *Phys. Rev. Lett.* **96**, 047207 (2006).

<sup>16</sup>B. Binz, A. Vishwanath, and V. Aji, *Phys. Rev. Lett.* **96**, 207202 (2006); B. Binz and A. Vishwanath, *Phys. Rev. B* **74**, 214408 (2006).

<sup>17</sup>U. K. Rößler, A. N. Bogdanov, and C. Pfleiderer, *Nature (London)* **442**, 797 (2006).

<sup>18</sup>I. Fischer, N. Shah, and A. Rosch, *Phys. Rev. B* **77**, 024415 (2008).

<sup>19</sup>B. Binz and A. Vishwanath, *Physica B* **403**, 1336 (2008).

<sup>20</sup>P. Bak and M. Høgh Jensen, *J. Phys. C* **13**, L881 (1980).

<sup>21</sup>J. M. Hopkinson and H.-Y. Kee, *Phys. Rev. B* **79**, 014421 (2009).

<sup>22</sup>E. Y. Vedmedenko, L. Udvardi, P. Weinberger, and R. Wiesendanger, *Phys. Rev. B* **75**, 104431 (2007); L. Udvardi, A. Antal, L. Szunyogh, A. Buruzs, and P. Weinberger, *Physica B* **403**, 402 (2008).

<sup>23</sup>N. Nagaosa, *J. Phys. Soc. Jpn.* **75**, 042001 (2006).

<sup>24</sup>K. Taguchi and G. Tatara, *Phys. Rev. B* **79**, 054423 (2009).